Graphene oxide-filled conducting polyaniline composites as methanol-sensing materials

Surajit Konwer · Ankur Kanti Guha · Swapan K. Dolui

Abstract Polyaniline/graphene oxide (PANI/GO) composites were prepared by polymerization of aniline monomer in the presence of GO under acidic conditions. The synthesized samples were characterized by Fourier transform infra red spectroscopy, ultraviolet–visible absorption, Raman spectroscopy, X-ray diffraction, scanning electron microscopy, transmission electron microscopy and thermogravimetric analysis. The direct current electrical conductivity of the composite was calculated by a four-probe technique. It is found that the conductivity dramatically increased to 241 S m^{-1} for PANI/GO (5 wt%) composite at 110 °C compared to pure PANI (7.5 S m^{-1}). The composite material was investigated as a methanol vapour sensor and compared with pure PANI. The methanol-sensing characteristics of the prepared composite was monitored by measuring the change in electrical resistivity on exposure to methanol vapour at different concentrations. The resistivity of PANI increases on exposure to methanol vapour because of strong hydrogen bonding between methanol with the polymer chain. A density functional theory study was carried out to verify the proposed concept of hydrogen bonding between the polymer chains and methanol. The presence of GO in PANI/GO composite increases the sensitivity towards methanol as compared with the pure PANI.

S. Konwer · A. K. Guha · S. K. Dolui
Department of Chemical Sciences, Tezpur University,
Tezpur 784028, Assam, India

S. Konwer
Department of Chemistry, Gargaon College, Sivasagar 785686,
Assam, India

S. Konwer (✉)
Department of Chemistry, Gargaon College, Simaluguri 785685,
Assam, India
e-mail: ksurajit27@gmail.com

Introduction

In recent years, attention has been given to the potential application of polyaniline (PANI) in chemical and biological sensors due to its high yield in redox process, gas sensing ability, optimum performance at room temperature, response to a wide range of volatile organic compounds (VOCs) environmental stability, etc. [1–4]. The detection of polluted gases, mainly toxic gases, is important to get clean the environment. Owing to the ability of PANI to undergo physiabsorb or chemisorb with the various VOCs and undergo swelling or redox reactions results in change in the resistance. Therefore, conducting PANI has been used as a sensing material for different gases where the effect of these gases on the electronic properties of these gases has been investigated [5–7].

Recently, graphene oxide (GO), a two-dimensional nanosheet of covalently bonded carbon atoms bearing various oxygen functional groups (e.g. hydroxyl, epoxide and carbonyl groups) on their basal planes and edges, has received a rapidly growing research interest [8–14]. Meanwhile, these oxygen-containing groups impart GO sheets with the function of strong interaction with polar small molecules or polymers to form GO-intercalated or exfoliated composites [15–22]. The thermal stability [15–18] and electrical properties [19, 20] of polymers could be greatly improved by the incorporation of GO nanosheets. In addition, a large number of polymer-GO or clay nanocomposites have become accessible in the form of end-functionalized derivatives because of small particle sizes and intercalation properties [21, 22]. Therefore, the potential of using GO-based materials for various applications such as supercapacitor, sensor, etc., has attracted much attention very recently [23–27].

The detection of polluted gases, especially toxic gases are important to get clean the environment. There have

been a great number of reports on the application of PANI and its composites in the detection of a wide spectrum of chemical substances including $CHCl_3$, NH_3, CO_2, hydrazine, vapours of common organic solvents, etc., by taking advantage of the variation of its electrical or optical properties on interaction with these chemical substances [1, 28–34]. Parmar and Rajanna [35] reported on Copper (II) oxide thin film for methanol and ethanol sensing. The maximum sensitivity observed for 2,500 ppm methanol and ethanol is 29 and 15.4 %, respectively. Faisal et al. [36] synthesized ZnO nanoparticles by hydrothermal treatment and reported that these ZnO thin film exhibits good sensitivity (0.9554 $\mu A\ cm^{-2}\ mM^{-1}$) towards detection of methanol at room conditions. Miao et al. [37] reported that the nickel-palladium nanoparticles showed the methanol sensitivity up to 0.168 $mAmM^{-1}$ and the detection limit was 12 μM.

Few reports are available that account for the use of PANI as a sensor for alcohol vapours, especially methanol, ethanol and propanol [35–44]. The alcohol vapour is one of the most extensively studied gases for these types of sensors materials. The alcohol vapours also popular gases in industry and day to day life so it is important to detect and control particularly due to the need for mobile practical devices to detect alcohol on the human breath or to detect leaks in distribution lines of industry. The PANI-based sensors exhibited good sensing properties such as ultrahigh sensitivity, fast response, satisfying reversibility, etc., and are suitable for practical applications. To the best of our knowledge, this is the first attempt to study such GO filled PANI composite for alcohol sensing applications.

In this study, the detailed study is performed on the static sensing behaviour of PANI/GO composites for methanol as well as ethanol and propanol in different analyte concentrations. This study also describes the preparation of PANI/GO composite by the incorporation of GO into PANI through the in situ polymerization of aniline. The sensitivity of the composite has been explained on the basis of the change in resistivity on exposure to alcohol vapours. In addition to this, the dependency of sensing response time as well as recovery time on the analyte concentration has also been reported.

Experimental

Materials

Aniline was obtained from Aldrich Co. and used without further purification. The natural graphite flake of size (crystalline, 300 mesh, Alfa Aesar) from Shanker Graphites and Chemical, New Delhi, India, hydrochloric acid (HCl), sulphuric acid (H_2SO_4), nitric acid (HNO_3), sodium nitrate

(NaNO$_3$), potassium permanganate ($KMnO_4$), hydrogen peroxide (H_2O_2) and potassium persulphate ($K_2S_2O_8$) were of analytical reagent grade chemicals (Merck) and used as received. Acetonitrile was obtained from Merck and purified by standard methods. For all purposes double distilled water was used.

Preparation of graphene oxide

GO was synthesized from natural graphite by a modified Hummers method described elsewhere [45]. In a 500-mL beaker, 5 g of graphite and 2.5 g of NaNO$_3$ were mixed with 120 mL of concentrated H_2SO_4. The mixture was stirred for 30 min at the temperature range of 0–5 °C. During stirring 15 g of $KMnO_4$ was slowly added to the suspension and the temperature was maintain to below 20 °C. After the addition of $KMnO_4$ the reaction mixture was then stirred at 30 °C until the mixture became pasty, and the colour turned into light brownish. Finally, 150 mL of H_2O was slowly added to the pasty with vigorous stirring. The diluted yellow colour suspension was again stirred at 98 °C for 24 h. Finally, 50 mL of 30 % H_2O_2 was added. The whole reaction mixture was washed by centrifugation with 1.5 M HCl and distilled water for 8–10 times and filtered to get the grey colour GO sheets.

Preparation of PANI/GO composites

PANI/GO composites were prepared by in situ polymerization of aniline in a suspension of GO in acidic solution. Typically, aniline was dissolved in 1 M HCl and 5 % GO particles (w/v) was dispersed in the resulting solution by bath sonicating for 1 h. While maintaining vigorous stirring at room temperature, another solution of $K_2S_2O_8$ with a mole ratio to aniline of 1:4 in 1 M HCl was rapidly poured to the mixture. Polymerization of aniline started after about 5 min, while the colour of the mixture changed into green. The mixture was allowed to stir at room temperature overnight and then diluted by 100 mL of water. The composites were collected by filtration and repetitively washed with water and ethanol until the filtrate become colourless.

Pure PANI was also synthesized by adopting the procedure as described above in the absence of GO in the reaction mixture.

Characterization

Fourier transform infrared spectroscopy (FTIR) was used to record FTIR spectra by Impact 410, Nicolet, USA, using KBr pellets. The ultraviolet–visible (UV–Vis) absorption spectroscopy of the samples in 1-methyl-2-pyrrolidon solvent was recorded using Shimadzu UV-2550 UV–Vis

spectrophotometer in the range of 300–800 nm. Raman spectra were recorded using a Nanofinder 30 confocal Raman with He–Ne laser beam having a wave length of 532 nm using a CCD detector. The surface morphology of the composites was observed using scanning electron microscope (SEM) of model JSM-6390LV, JEOL, Japan. The surface of the sample was coated with platinum before SEM analysis. Transmission electron microscope (TEM) measurements were conducted on a PHILIPS CM 200 microscope at 200 kV. The TEM samples were prepared by dispensing a small amount of dry powder in ethanol. Then, one drop of the suspension was dropped on 300-mesh copper TEM grids covered with thin amorphous carbon films. To study the thermal degradation of the samples, thermogravimetric analysis (TGA) was performed using TG 50, Simadzu thermogravimetric analyser, Japan from temperature range 298–973 K with a heating rate of 10 °C min^{-1} under the nitrogen flow rate of 30 mL min^{-1}. The X-ray diffraction (XRD) study was carried out at room temperature (ca. 298 K) on Rigaku X-ray diffractometer with CuKα radiation ($\lambda = 0.15418$ nm) at 30 kV and 15 mA using a scanning rate of 0.050° s^{-1} in the range of $2\theta = (10–70)°$. Using a compression-moulding machine, pellets of composite samples were made. High pressure was applied (1.5–2 ton) to the sample to get hard round-shaped pellet (1.5-cm diameter, 2-mm breadth), which was used to measure the electrical conductivity. The sample was put on the base plate of the four-probe arrangement and the probes were rested gently on the surface of the pellet sample for directly measured the conductivity. The four-probe arrangement was then connected with a PID-controlled oven. The digital microvoltmeter mode was then adjusted to voltage measuring mode and the voltage between the probes was measured. Finally, the oven was on and the rate of heating can be chosen between low and high as desired. The voltage of sample was collected in the temperature range of 25–150 °C.

DFT calculation was performed by Gaussian 03 suite of program [46] to determine the interaction between the bare polymer and the methanol vapour.

Sensor testing measurements

The methanol vapour sensing property of PANI/GO composite was studied using a gas-sensor setup as shown in Fig. 1. The PANI/GO composite pellet was placed in an oven for 24 h at 80 °C to remove excess solvent present in the composite material. The pellet was placed into the glass chamber and the contact between the sensor (as pellets) and the two probes was made with the help of silver paste. The change in resistance was measured using a two probe Keithley 2400 source meter by means of labtracer software at the room temperature at the scan rate 0.1 V s^{-1}. Hexane
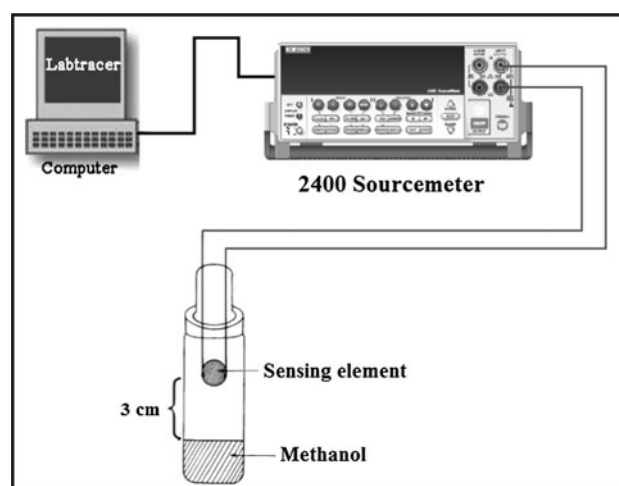

Fig. 1 Methanol vapour sensor setup

was used as a diluent to obtain different concentration of the alcohol vapours. The distance between sensing material and solvent was kept 3 cm at the time of exposure of different concentration of methanol on the sensing material. The sensing ability of the composite was investigated by recording the electrical responses when exposed alternately to different concentration of alcohol vapour at room temperature and withdrawing the sensor from the analyte molecule to recover the sensor.

Results and discussion

The PANI/GO composite was prepared by in situ oxidative polymerization. The monomer aniline may get adsorbed on the surface and gallery of GO. This adsorbed aniline on GO as well as remaining free aniline gets polymerized in the presence of oxidizing agent $K_2S_2O_8$ to yield PANI/GO composite. The possible H-bonding between GO and PANI in the PANI/GO composite is schematically depicted in Fig. 2. The functional groups, –OH, –COOH and epoxy, exist on the surface and pores of the GO which promote the hydrogen bonds between the GO to amine and imine nitrogen of benzenoid and quinoid moieties of the polymer chain. It is also expected that there would be π–π stacking between the polymer backbone and the GO sheets [47].

FTIR analysis

The FTIR spectra of GO, PANI, unexposed PANI/GO and methanol-exposed PANI/GO is shown in Fig. 3. For the PANI powder sample, the absorption peak at 3430 cm^{-1} is attributable to the N–H stretching vibrations of the leuco-emeraldine component [4]. The weak peak at 2924 cm^{-1} corresponds to aromatic sp^2 CH stretching. The absorption
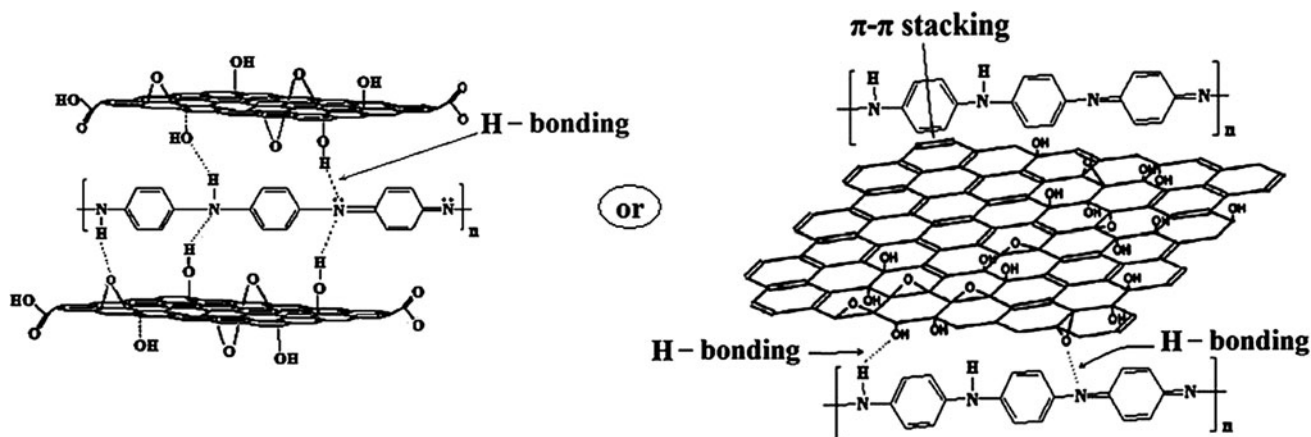
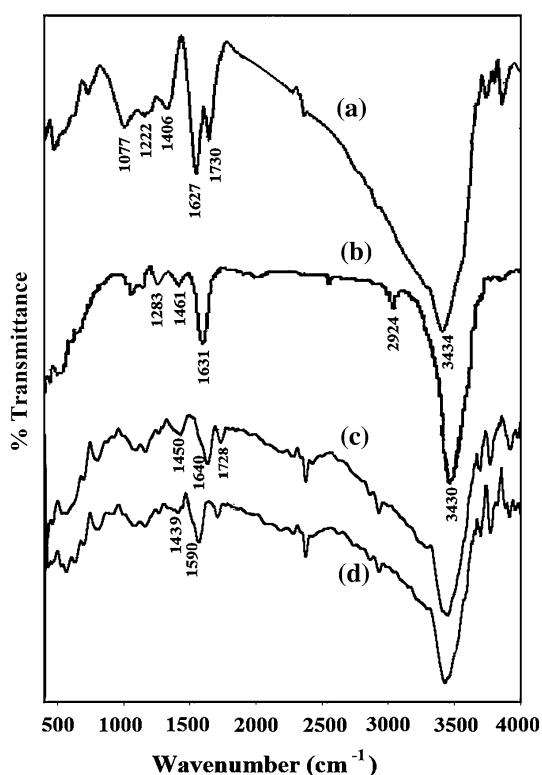**Fig. 2** Schematic presentation depicting interaction of GO sheet and PANI chain

Fig. 3 FTIR spectra of *a* GO, *b* PANI, *c* PANI/GO in air and *d* PANI/GO with methanol
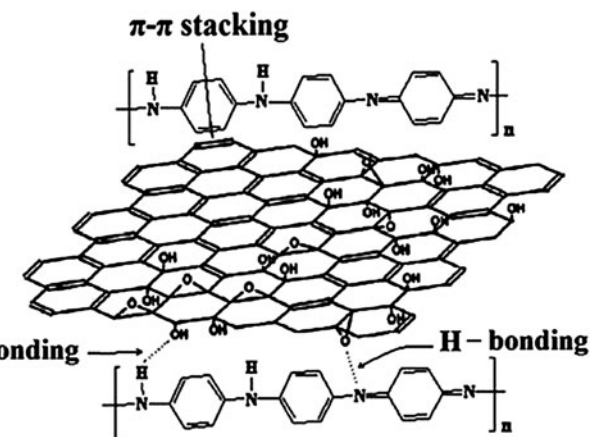

Fig. 4 UV–Vis spectra of *a* GO, *b* PANI/GO composite and *c* pure PANI

1077 cm^{-1}. By comparison, the spectrum of the PANI/GO composites, the absorption peaks are similar to PANI except that the characteristic peak of C=O group at 1728 cm^{-1} was observed from PANI/GO composite. The absorption peaks at ~ 1640 and 1450 cm^{-1} represent the quinoid and benzenoid structures of the PANI in unexposed PANI/GO composite [50]. A comparison of the FTIR spectra of the methanol-exposed PANI/GO composite reveal that the benzenoid and quinoid peak is shifted from 1450 to 1439 cm^{-1} and 1640 to 1590 cm^{-1}, respectively. This can be attributed to the interaction (probably H-bonding) in between the methanol and benzenoid and quinoid nitrogens of the polymer chain, thereby causing the reducing effect. The presence of PANI characteristic vibrations, suggesting PANI, can be successfully deposited on the GO surface.

UV analysis

Figure 4 represents the UV–Vis absorption spectra of the PANI, GO and PANI/GO composite recorded in NMP.

peaks located at 1631 and 1461 cm^{-1} are ascribed to the C=C stretching deformation of the quinoid ring in the emeraldine salt and benzenoid rings leucoemeraldine [48]. The peaks at 1283 and 1152 cm^{-1} correspond to C–N stretching of the secondary aromatic amine and C=N stretching, respectively [49]. For the GO, the characteristic vibrations include the broad and intense O–H peak at 3434 cm^{-1}, strong C=O peak in carboxylic acid and carbonyl moieties at 1730 cm^{-1}, C–OH peak at 1406 cm^{-1}, C–O–C peak at 1222 cm^{-1}, C–O stretching peak at

The UV–Vis spectrum of PANI shows an intense absorption peak at 220 nm, a weak peak at 270 nm and a broad peak at 425 nm. The first and second absorption bands are related to the molecular conjugation (π–π^* transition), while the third absorption peak assigned to the polaron state of PANI, i.e. charged cationic species. The sharp UV–Vis spectrum of GO was observed at 235 nm. The PANI/GO composite shows similar spectrum with pure PANI where the spectrum at 425 nm is shifted to 415 nm, indicating that PANI was also in the polaronic state in the synthesized PANI/GO composite. Moreover, the two peaks at 215 and 280 nm were related to the molecule conjugation. However, all the three PANI band in PANI/GO is shifted due to the interaction of polymer chain and GO sheets.

Raman analysis

As a non-destructive tool, Raman spectroscopy is often used to evaluate the qualitative and quantitative analyses of carbon products microscopically [51]. The Raman spectra for the PANI/GO nanocomposite and GO are shown in Fig. 5. The Raman spectrum of GO shows two characteristic peaks at 1335 and 1565 cm^{-1} correspond to the D and G bands [47, 52]. The D band corresponded to the defects or edge areas and disordered carbon, whereas the G band arises from the zone centre E_{2g} mode, corresponding to the vibration of sp^2-hybridized carbon. Additionally, the D band is related to the edge, structural defects which correspond to the conversion of a sp^2-hybridized carbon to a sp^3-hybridized carbon. The intensity ratio (ID/IG) between the D band and G band is found to be 0.80 for pure GO which indicates a high level of disorder of the GO layers due to the oxidation of graphite. In the Raman spectra of the PANI/GO composite, the Raman-active bands with the D band shift to 1358 cm^{-1} and the G band to 1583 cm^{-1} which reveals π–π interaction between the PANI and the
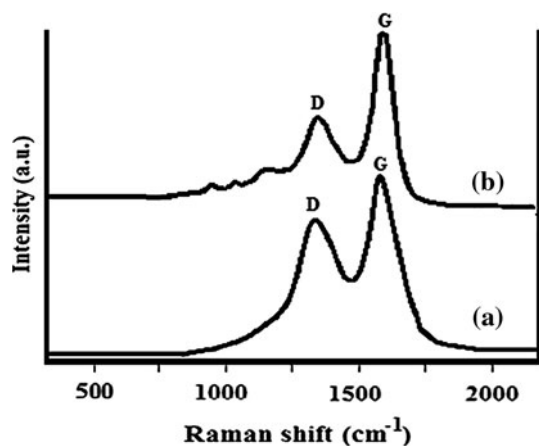
GO sheets. Additionally, the spectrum of PANI shows a broad band at 1175 cm^{-1} and two small bands at 1050 and 930 cm^{-1} corresponding to C–H bending of the quinoid ring, C–N$^+$ stretching of the bipolaron and polaron structure of PANI structure. Thus, Raman spectra of the composite show the bands related to both of their PANI and GO components. This is in good agreement with FTIR results [53].

XRD analysis

Figure 6 shows the XRD pattern of pure PANI, GO and PANI/GO composite. The XRD pattern of pure PANI, which had a broad peak at about $2\theta = 25.8°$, a characteristic peak of amorphous PANI. In GO, a broad reflection with peak at $2\theta = 13.1$ Å has been observed, which is similar to that reported in the earlier literature. This indicates the formation of layer-like GO sheets. The PANI/GO composite exhibits two peaks at $2\theta = 13.2°$ for GO and $2\theta = 25.82°$ for PANI. This shows the incorporation of GO into the PANI matrix.

Thermogravimetric analysis

Thermogravimetric profiles of PANI, GO and PANI/GO composites are given in Fig. 7. The initial weight loss for all the samples at temperature range of 90–115 °C reveals the loss of moisture from the polymer matrix. The major degradation occurs at 310 °C for PANI, while the major weight loss of GO at the temperature range of 215–310 °C

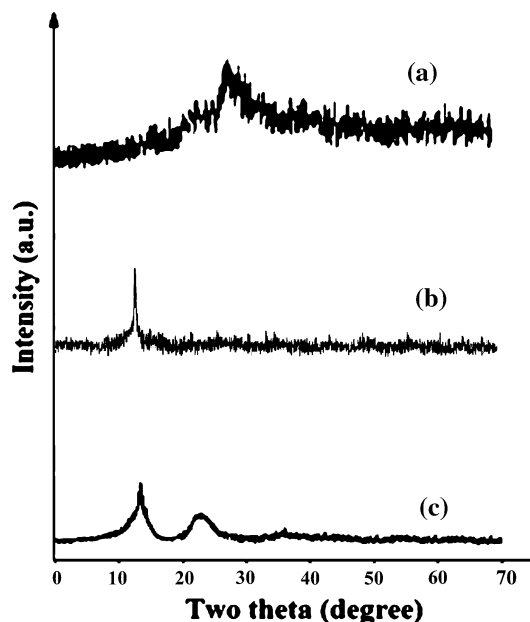Fig. 6 XRD analysis of *a* pure PANI, *b* GO and *c* PANI/GO composite

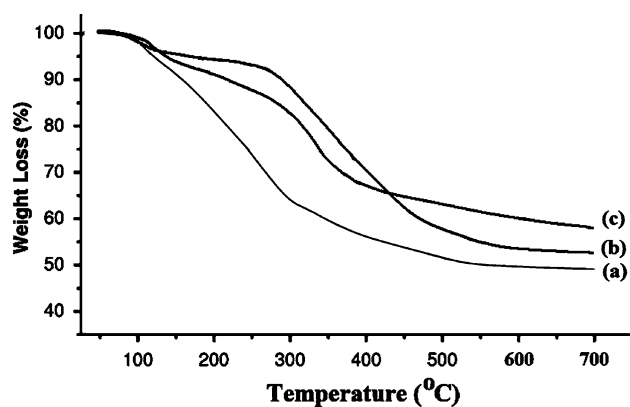Fig. 5 Raman spectra of *a* GO and *b* PANI/GO composite

Fig. 7 TGA of *a* GO, *b* PANI/GO composite and *c* PANI

reveals the decomposition of oxygen-containing functional groups[45, 54]. In PANI/GO composite, a mass loss of 15 % can be observed from 125 to 300 °C.

SEM analysis

SEM images of the pure PANI, GO and PANI/GO are shown in Fig. 8. The GO inherits the layer-by-layer and network structure, but in a denser stacking, compared with the randomly aggregate structure having rough surface for the pure PANI is observed. In the SEM micrographs of

PANI/GO composite, smooth surfaces are observed. Since the polymers are grown in the pores and galleries of GO, it is difficult to distinguish the individual phase, i.e. GO and PANI in PANI/GO composite from the SEM micrograph.

TEM analysis

Typical morphology of GO is shown in the TEM image of Fig. 9a. The GO prepared here has a typically curved, layer-like structure with thickness of ∼5–10 nm of thinner. For PANI/GO composite (Fig. 9b), TEM image shows that all the GO sheets are homogeneously coated with PANI and the PANI mainly grown on the surface or intercalate between the GO sheets. SEM and TEM images reveal that the chemically modified GO and the PANI formed a uniform composite with the PANI absorbed on the GO surface and/or filled between the GO nanosheets.

DC electrical conductivity

DC electrical conductivity of conducting composite is measured using a four-probe resistivity measurement system. The conductivity of PANI/GO composite was calculated by the following equations:
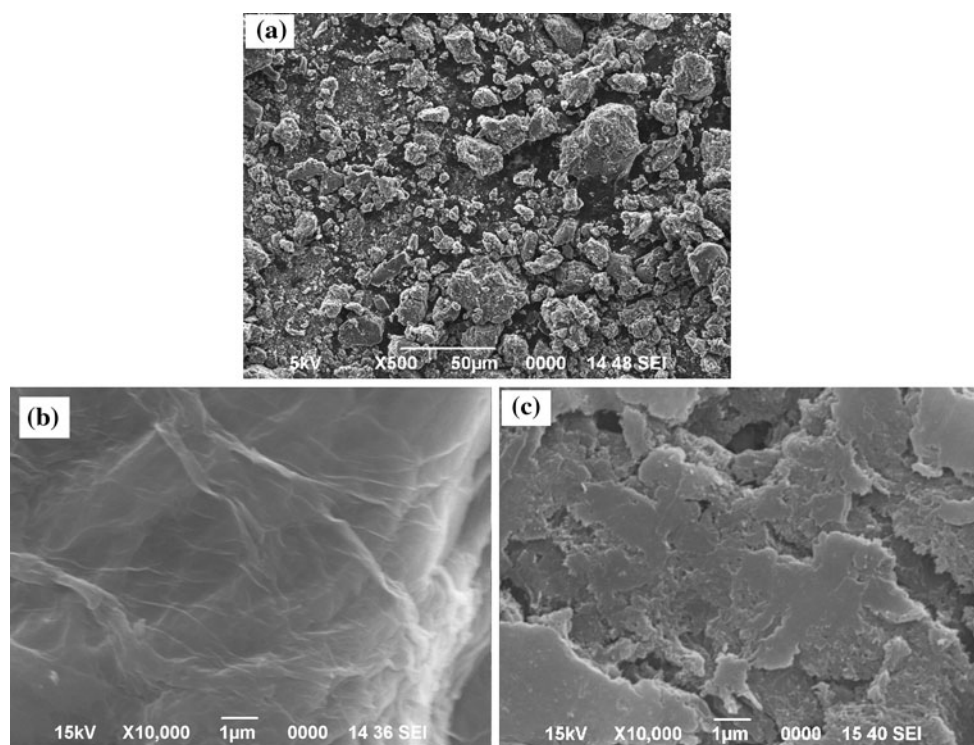

Fig. 8 SEM images of **a** PANI **b** GO and **c** PANI/GO composite
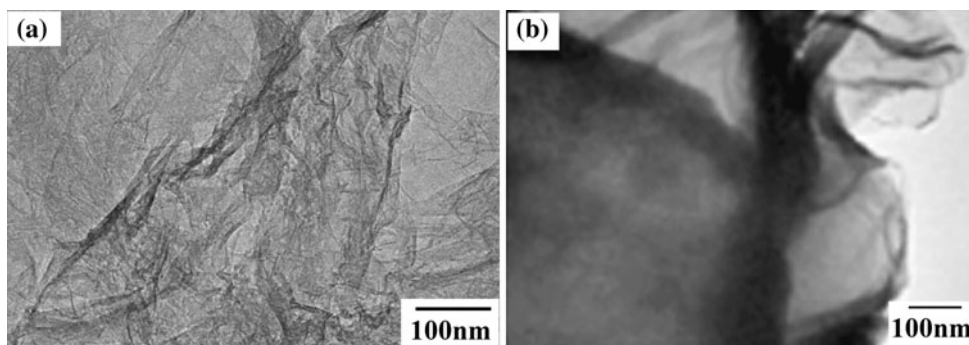
Fig. 9 TEM images of **a** GO and **b** PANI/GO composite

Table 1 Conductivity of the PA and PA/GO composite at various temperatures

Temperature (°C)	Conductivity (S m^{-1})		
	GO	PA	PA/GO
25	0.5	5	178
30	–	5	178
50	–	6.5	185
70	–	7.3	201
90	–	7.3	230
110	–	7.5	241
130	–	7.5	241
150	–	7.5	241

$$\rho = \rho_o / G_7(W/S) \qquad (1)$$

$$G_7(W/S) = (2S/W)\ln 2 \qquad (2)$$

$$\rho_o = (V/I)2\pi S \qquad (3)$$

$$\sigma = 1/\rho_o \qquad (4)$$

Where $G_7(W/S)$ is a correction divisor which is a function of thickness of the sample as well as probe-spacing; I, V, W and S are current (A), voltage (V), thickness of the pellet (cm) and probe-spacing (cm), respectively.

The electrical conductivities of the PANI, GO and the composite material is determined and the conductivities are listed in Table 1. The GO sample shows a low conductivity of 0.5 S m^{-1} similar to that reported in the earlier literature [55]. The PANI sample shows conducting behaviour with the maximum conductivity of 7.5 S m^{-1}. However, the dc electrical conductivity of the PANI/GO composite (178–241 S m^{-1}) is increased dramatically in comparison to that of PANI and GO alone. This type dramatic enhancement of electrical conductivity of PA/GO composite after incorporation of GO into PA has also been found in earlier literature [45]. Such enormous enhancement of the conductivity of PANI/GO composite might be attributed to the π–π stacking between the polymer backbone and the GO sheets. (Fig. 2). Moreover, the
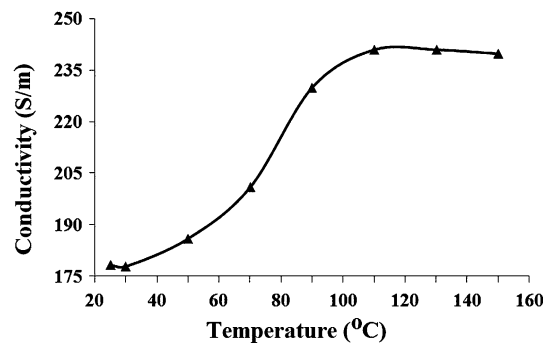

Fig. 10 Temperature dependence of electrical conductivity of PANI/GO composite

polymerization on the surface and pores of GO sheets restricts the twisting of the polymer backbone away from its planarity which plays a major role to enhance the conductivity. Therefore, GO is the most effective in imparting the conductivity.

The electrical conductivity of PANI and PANI/GO composite is also measured in the temperature range of 25–150 °C. The electrical conductivity increases with temperature showing semi-conducting behaviour and the maximum conductivity is found to be 241 S m^{-1} for PANI/GO (5 wt%) at 110 °C and after that no deviation in conductivity was observed (Fig. 10). At high temperature, the mobility of the charge carrier increases with the increase in inter- and intra-chain hoping. An increase in inter- and intra-chain hopping results in a high charge carrier mobility within the composite, which leads to an increase in the conductivity at appropriate high temperatures [9, 26, 56].

Sensor behaviour

To carry out the sensing ability of the pure PANI and PANI/GO composite, we have studied the changes in the electrical response of the pure PANI and composite material on exposing to different concentrations of methanol vapours. The electrical response is expressed in terms of sensitivity, $\Delta R/R_0$. Figure 11 depicts the sensitivity
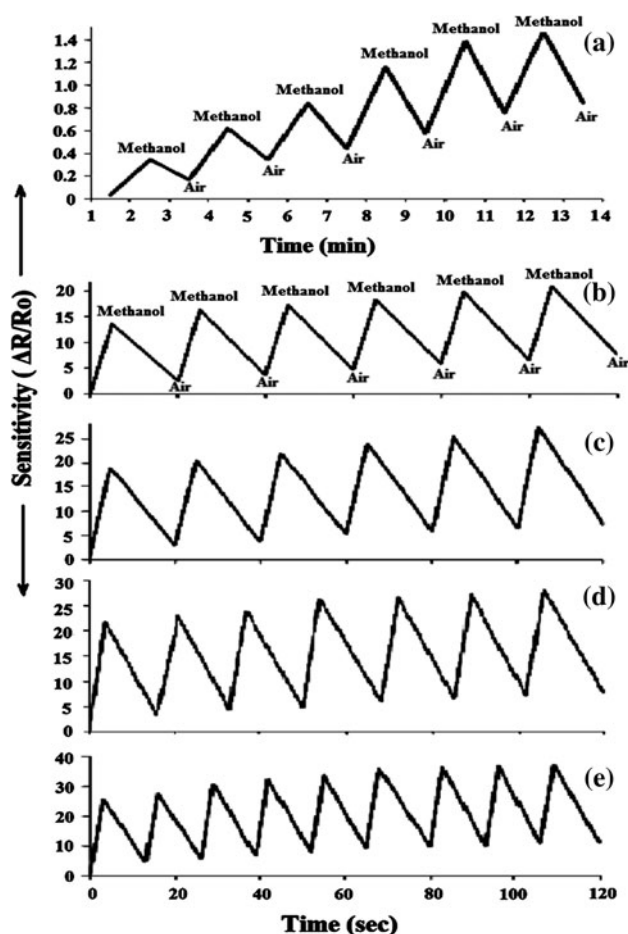
Fig. 11 Response curves of **a** pure PANI and PANI/GO exposed to saturated vapours of methanol at different concentrations **b** 100 ppm, **c** 200 ppm, **d** 300 ppm and **e** 500 ppm

($\Delta R/R_0$), obtained from the pure PANI and the PANI/GO composite exposed to different concentrations of methanol vapours in the concentration of 100–500 ppm. Here, the sensitivity is defined as

$$\Delta R/R_0 = R - R_0/R_0 \qquad (5)$$

where, R_0 and R are the initial resistance of sensor in air and in target gas, respectively.

PANI is a p-type semiconductor, the exposure to electron-donating gases, such as methanol vapours, will cause an increase in the resistance [57]. This is in good agreement with our experimental results. When pure PANI is exposed to methanol vapour to for 2.5 min, it shows a change in the $\Delta R/R_0$ value from 0.03 to 0.35 and on removal of methanol vapour the $\Delta R/R_0$ value decreased to 0.17, i.e. the $\Delta R/R_0$ does not revert to initial state on removal of the analyte methanol. Similarly, the changes in $\Delta R/R_0$ values for subsequent cycles are gradually increasing and after each cycle, the base line of $\Delta R/R_0$ versus time curve does not get back to the initial state. This gradual shift indicates the irreversible sensing character of the pure

PANI. Additionally, it is found that the recovery time is more than that of response time (Fig. 11a). This may be due to the physical absorption as well as the H-bonding in between methanol vapours and the benzenoid and quinoid moiety of PANI backbone. We have carried out DFT study to confirm this assertion of H-bonding with the amine and imine nitrogen of benzenoid and quinoid moieties of the polymer chain and methanol. The sensitivity ($\Delta R/R_0$) of pure PANI to methanol is found in the range of 0.35–1.47 within 2–15 min on exposure to methanol vapour.

In PANI/GO composite, it is observed that the sensing property is better and reproducible than pure PANI (Fig. 11b, e). When PANI/GO is exposed to the methanol the sensitivity ($\Delta R/R_0$) increasing with very short time period (3–120 s) and on removal of the methanol vapours it get back to its original state with slight deviation indicates the better reversible character. Here, the recovery time to release methanol from PANI/GO composites is almost same with the response time. This may be due to the physical as well as chemical interaction of the PANI, GO and methanol vapours. When PANI/GO composite is exposed to methanol, strong H-bonding takes place between the methanol vapour with the bare polymer and GO, thereby disrupting the extended H-bonding between GO and PANI back bond. This results in the enhancement of resistivity (Fig. 12). After the removal of methanol vapours, possible reformation of the extended H-bonding between GO and PANI is taking place and restore the original H-bonded PANI/GO composite. Thus, the presence of GO imparts rapid response and reversible character of the sensor. These results are further supported by the FTIR study. In PANI/GO composite, the sensitivity increases with increase in the gas concentration and maximum sensitivity $\Delta R/R_0$ are shown up to 37 for 500 ppm methanol.

The responses of PANI/GO sensor pellet for the ethanol and propanol are also investigated and shown in Fig. 13. The sensitivities ($\Delta R/R_0 = 3.77$ and 3.1) are less towards ethanol and propanol vapours due to the low polarity nature of these two alcohols compared to the methanol. On the other hand, the response and recovery time for both ethanol and propanol is also increased because the methanol is more polar and small in size than ethanol and propanol; hence, it would interact more efficiently than the other two alcohols. The selectivity of PANI/GO composite with respect to these three alcohols are as methanol $\ll$ ethanol $<$ propanol.

The density functional study has been carried out using B3LYP/6-31+G* level of theory [57–59]. This is a hybrid of Hartree–Fock and density functional theory based on generalized gradient approximation (GGA). The advantage of using GGA is that it will not lead to strong bonding of the molecules as in local density approximation. Hence, if
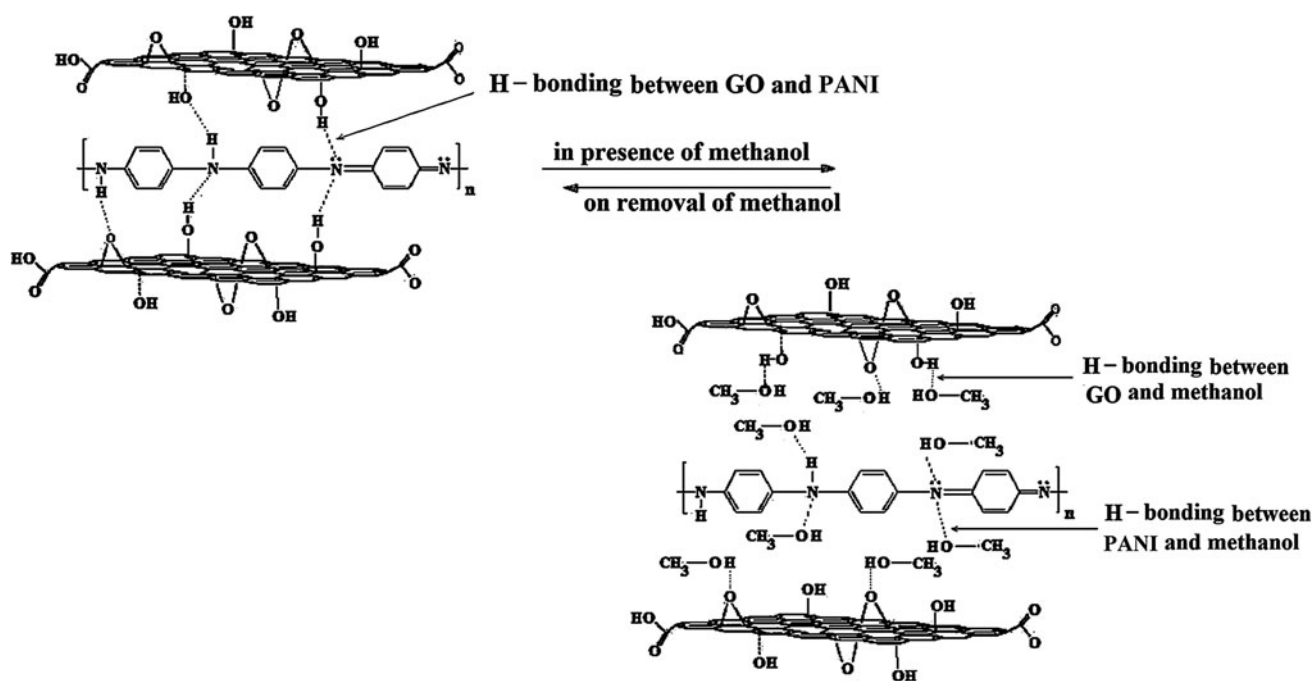
Fig. 12 Schematic presentation depicting interaction of methanol vapours with PANI/GO composite
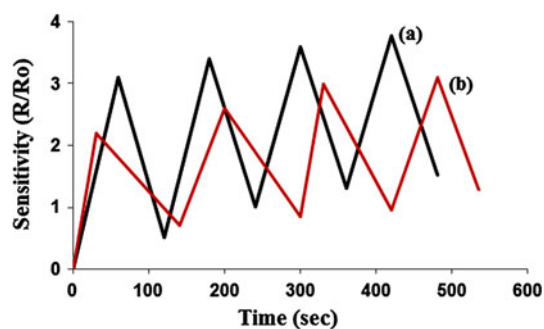

Fig. 13 Response curves of PANI/GO composite exposed to saturated vapours of *a* ethanol and *b* propanol

Fig. 14 DFT-optimized geometry of the bare polymer and methanol showing the possibility of H-bonding

GGA shows any bonding, it is confirmed that they will bind in the real system. The binding or the complexation energy between methanol and PANI is 3.5 kcal mol^{-1}. The optimized geometry of the molecule shows that the distance of the –OH hydrogen of the methanol molecule from the imine nitrogen atom of the quinoid moieties is 2.009 Å and the distance of the amine hydrogen atom of benzenoid moieties and the oxygen atom of methanol molecule is 1.976 Å (Fig. 14), thus confirming the presence of H-bonding between the polymer chain and methanol vapour. This hydrogen bonding shifts the –NH stretching frequencies of benzenoid and quinoid ring of the polymer as is evident from FTIR analysis. Further, the presence of methanol vapour in a close proximity to the polymer twists the PANI away from planarity as evident in the optimized geometry which is responsible for the increase in resistivity.
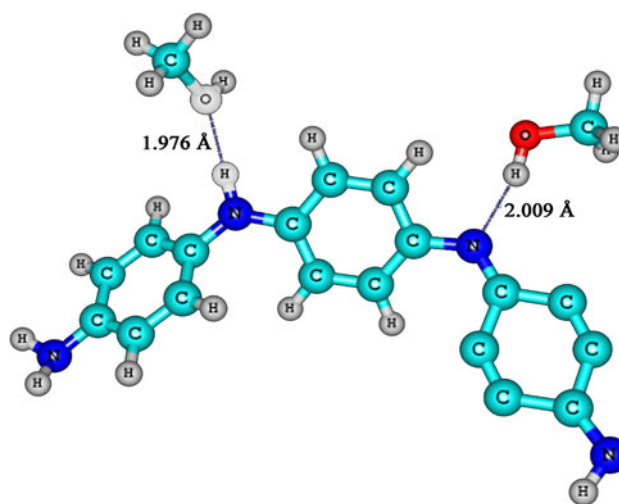
The comparison of the sensitivity of PANI/GO composite sensor and pure PANI sensor is shown in Fig. 15. The PANI/GO composite sensors pellet shows the sensitivity limit with methanol vapour concentration up to 500 ppm, and thereafter the sensitivity became saturated. The PANI/GO composite sensor shows higher sensitivity ($\Delta R/R_0 = 13.6–37$) in all range of vapour concentrations than that of pure PANI ($\Delta R/R_0 = 0.35–1.47$). This may be due to the large specific surface area of GO-sheet present in the PANI/GO composite where the maximum surface absorption can be possible.
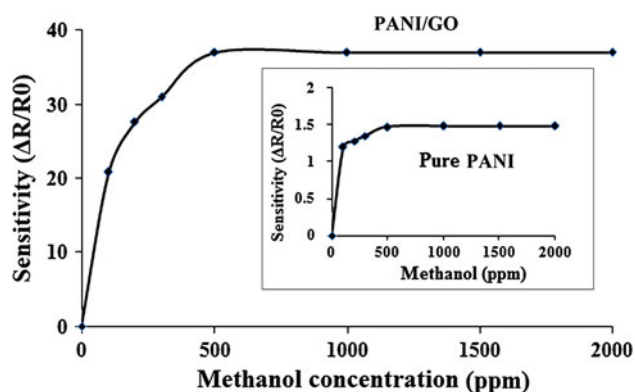
Fig. 15 Actual response curves of *a* Pure PANI and *b* PANI/GO with various concentrations of methanol vapours

Conclusions

GO-filled PANI composite has been synthesized successfully. The DC electrical conductivity of the PANI/GO composite is much higher (241 S m^{-1}) in comparison with the pure PANI (7.5 S m^{-1}). On the basis of conducting behaviour of the material, three different alcohols, viz. methanol, ethanol and propanol sensing studies are performed. It is observed that the PANI/GO composite is found to be a highly sensitive ($\Delta R/R_0 = 20.9$–37) sensor material for methanol vapours (100–500 ppm) than that of ethanol ($\Delta R/R_0 = 3.77$) and propanol ($\Delta R/R_0 = 3.1$). The response time and reversibility of PANI/GO composite is much efficient that of pure PANI. The basic mechanism of the interaction between methanol and PANI is believed to be hydrogen bonding as revealed by DFT and FTIR studies. For the base polymer PANI, the H-bonding can occur via both the quinoid moieties' nitrogen and the –NH group of the benzenoid moieties to the hydrogen and oxygen atoms of the methanol's hydroxyl group, respectively. These observations paved the way of applicability of PANI/GO composite as a more efficient methanol sensor material.

References

1. Huang JX, Virji S, Weiller BH, Kaner RB (2003) J Am Chem Soc 125:314
2. Gurunathan T, Chepuri RKR, Narayan R, Raju KVSN (2012) J Mater Sci. doi:10.1007/s10853-012-6658-x
3. Maiti J, Pokhrel B, Boruah R, Dolui SK (2009) Sens Actuator B 141:447
4. Yan XB, Han ZJ, Yang Y, Tay BK (2007) Sens Actuators B 123:107
5. Chithralekha P, Balaji M, Subramanian S, Padiyan PD (2010) Curr Appl Phys 10:457
6. Xie D, Jiang Y, Pan W, Li D, Wu Z, Li Y (2002) Sens Actuators B 81:158
7. Kim JS, Sohn SO, Huh JS (2005) Sens Actuators B 108:409
8. Geim AK, Novoselov KS (2007) Nat Mater 6:183
9. Wu J, Pisula W, Mullen K (2007) Chem Rev 107:718
10. Bunch JS, van der Zande AM, Verbridge SS, Frank IW, Tanenbaum DM, Parpia JM, Craighead HG, McEuen PL (2007) Science 315:490
11. Jang BZ, Zhamu A (2008) J Mater Sci 43:5092. doi:10.1007/s10853-008-2755-2
12. Wang X, Zhi L, Mullen K (2008) Nano Lett 8:323
13. Jonathan P, Pandey PA, Moore JJ, Bates M, Kinloch IA, Young RJ, Wilson NR (2011) Angew Chem Int Ed 50:3173
14. Wilson NR, Pandey PA, Beanland R, Young RJ, Kinloch IA, Gong L, Liu Z, Suenaga K, Rourke JP, York SJ, Sloan J (2009) ACS Nano 3:2547
15. Matsuo Y, Tahara K, Sugie Y (1997) Carbon 35:113
16. Liu PG, Gong KC, Xiao P, Xiao M (2000) J Mater Chem 10(4):933
17. Xu JY, Hu Y, Song L, Wang QG, Fan WC, Liao GX et al (2001) Polym Degrad Stab 73:29
18. Kai WH, Hirota Y, Hua L, Inoue Y (2008) J Appl Polym Sci 107:1395
19. Kotov NA, Dekany I, Fendler JH (1996) Adv Mater 8:637
20. Cassagneau T, Fendler JH (1998) Adv Mater 10:877
21. Kovtyukhova NI, Ollivier PJ, Martin BR, Mallouk TE, Chizhik SA, Buzaneva EV et al (1999) Chem Mater 11:771
22. Wu JH, Tang QW, Sun H, Lin JM, Ao HY, Huang ML et al (2008) Langmuir 24:4800
23. Yan J, Wei T, Shao B, Fan QZ, Wei F et al (2010) Carbon 48:487
24. Futaba DN, Hata K, Yamada T, Hiraoka T, Hayamizu Y, Iijima S et al (2006) Nat Mater 5:987
25. Portet C, Chmiola J, Gogotsi Y, Park S, Lian K (2008) Electrochim Acta 53:7675
26. Yang CM, Kim YJ, Endo M, Kanoh H, Yudasaka M, Iijima S et al (2007) J Am Chem Soc 129:20
27. Zhang LL, Zhao XS (2009) Chem Soc Rev 38:2520
28. Nicolas-Debarnot D, Poncin-Epaillard F (2003) Anal Chim Acta 475:1
29. Prasad GK, Radhakrishnan TP, Kumar DS, Krishna MG (2005) Sens Actuators B 106:626
30. Tan CK, Blackwood DJ (2000) Sens Actuators B 71:184
31. Dixit V, Misra SCK, Sharma BS (2005) Sens Actuators B 104:90
32. Ogura K, Shiigi H (1999) Electrochem Solid State Lett 2:478
33. Chabukswar VV, Pethkar S, Athawale AA (2001) Sens Actuators B 77:657
34. Anitha G, Subramanian E (2003) Sens Actuators B 92:49
35. Parmar M, Rajanna K (2011) Int J Smart Sens Intell Syst 4:710
36. Faisal M, Khan SB, Rahman MM, Jamal A, Abdullah MM (2012) Appl Surf Sci 258:7515
37. Miao F, Tao B, Chu PK (2012) Anal Lett 45:1447
38. Santra S, Guha PK, Ali SZ, Hiralal P, Unalan HE, Covington JA et al (2010) Sens Actuators B 146:559
39. Barker PS, Chen JR, Agbor NI, Monkman AP, Mars P, Petty MC (1994) Sens Actuators B 17:143
40. Ogura K, Shiigi H, Nakayama M, Fujii A (1998) J Electrochem Soc 145:3351
41. MacDiarmid AG, Zhang WJ, Feng J, Haung F (1998) ANTEC' society of plastic engineers, Atlanta, pp 1330–1334
42. Sukeerthi S, Contractor AQ (1994) Indian J Chem Sect A 33:565
43. Hatfield JV, Neaves PI, Hicks PJ, Persuad KC, Travers P (1994) Sens Actuators B 18:221
44. Pradip K, Pradhan NC, Adhikari B (2009) Sens Actuators B 140:525
45. Zhang K, Zhang LL, Zhao XS, Wu J (2010) Chem Mater 22:1392

46. Frisch MJ, Trucks GW, Schlegel HB, Scuseria GE, Robb MA, Pople JA et al. (2003) Gaussian 03, revision D.02, Gaussian, Inc., Pittsburgh

47. Wang H, Hao Q, Yang X, Lu L, Wang X (2010) Appl Mater Interfaces 2:821

48. Cruz-Silva R, Romero-Garcia J, Angulo-Sanchez JL, Flores-Loyola E, Farias MH, Diaz JA et al (2004) Polymer 45:4711

49. Tiwaria A, Kumar R, Prabaharan M, Pandey RR, Kumari P, Mishra AK et al (2010) Polym Adv Technol 21:615

50. Huang WS, MacDiarmid AG (1993) Polymer 34:1833

51. Yong D, Shirley ZS, Weidong Y, Richard D, Kefeng C, Philip SC (2012) Synth Met 161:2688

52. Kudin KN, Ozbas B, Schniepp HC, Prud'homme RK, Aksay IA, Car R (2008) Nano Lett 8:36

53. Zhang D, Zhang X, Chen Y, Yu P, Wang C, Ma YJ (2011) Power Sources 196:5990

54. Gomez-Navarro C, Weitz RT, Bittner AM, Scolari M, Mews A, Kern K et al (2007) Nano Lett 7:3499

55. Konwer S, Dolui SK (2010) Mater Chem Phys 124:738

56. Miasik JJ, Hopper A, Tofield BC (1986) J Chem Soc Faraday Trans 82:1117

57. Becke AD (1993) J Chem Phys 98:5648

58. Lee C, Yang W, Parr RG (1988) Phys Rev B 37:785

59. Vosko SH, Wilk L, Nusair M (1980) Can J Phys 58:1200